Astron. Astrophys. 253, 586–600 (1992)

ASTRONOMY AND ASTROPHYSICS

Acoustic waves in the solar atmosphere IX

Three minute pulsations driven by shock overtaking

Wolfgang Rammacher and Peter Ulmschneider

Institut für Theoretische Astrophysik, Universität Heidelberg, Im Neuenheimer Feld 561, W–6900 Heidelberg, Federal Republic of Germany

Received July 15, accepted September 14, 1991

Abstract. We show that short-period acoustic waves with periods less than 40 s, by the process of shock overtaking, are able to drive three minute type first overtone pulsations of the solar chromosphere. Waves with such periods are the main driving mechanism for these pulsations which receive of the order of 50 percent of the available wave energy. Simulations of the Mg II k and Ca II K line profiles show a very similar emission core evolution as is observed for Ca II K_{2V} cell grains.

Key words: hydrodynamics – shocks – pulsations – solar chromosphere – chromospheric line emission

1. Introduction

After about a decade of calm in the literature an intense attention has recently been given to two, probably connected solar phenomena: the Ca II K_{2V} cell grains and the chromospheric three minute oscillations. This research culminated in a review by Deubner (1991) and an even more extensive one by Rutten and Uitenbroek (1991). For this reason the phenomena are only briefly summarized here.

For the *three minute oscillations* a detailed account of the observed properties has recently been given by Fleck and Deubner (1989) as well as by Deubner and Fleck (1990). These authors determined auto and cross correlations of intensity and velocity fluctuations of high spatial resolution measurements of the Ca II infrared triplet lines at 8542Å and 8498Å, the Na D_1 line and photospheric Fe I lines. Due to a fast repetition rate and a long duration of the observations these measurements achieved a high temporal and spectral resolution.

The power spectra of the mentioned lines showed that the three min oscillations are a distinct phenomenon of the middle to high chromosphere (at heights greater than 800 km), visible only in the interior of the supergranulation cells: while the Na D_1 and the Fe lines showed power spectrum maxima at the familiar 300 s, the Ca IRT lines in the cell interior showed maxima at 166 to 180 s. Phase spectra of the velocity correlations of the Ca 8542Å and 8498Å lines revealed the signature of running waves with high phase speed. Yet velocity-intensity correlations of the same lines showed 90^0 phase shifts for the entire spectrum from periods of 50 s to 180 s, which would be expected for standing waves. The phase spectra of velocity correlations between the Ca and Fe lines indicated running waves which, however, could only be fitted to a theoretical spectrum when the height difference between the two line forming layers was reduced from the theoretical 1300 km to a value of 800 km.

Fleck and Deubner have interpreted these observations as a spectrum of propagating waves which at a "magic height" near 800 to 1000 km, runs into heavy damping and toward greater height becomes a spectrum of standing waves. Puzzling is the fact that at the height of the Ca IRT lines, which after this picture lies in the standing wave region, the familiar standing wave signature, constant phase and sudden 180^0 phase jumps, of which at least two are expected, has not been observed.

Ca II K_{2V} cell grains are intermittent emission phenomena in the interior of supergranulation cells. They are best seen in the cores of the Ca II H and K lines but they are also observed in the UV continuum at 1600 Å. UV and K_{2V} cell grains are probably the same phenomenon. The cell grains have a horizontal size of about 1 to 2 arcsec and a repetition time of about 160-180 s (Liu 1974). When one plots the emission core region of the Ca II lines as function of time, a characteristic emission core evolution is seen which has been displayed both by Deubner (1991, Fig. 2) and by Rutten and Uitenbroek (1991, Fig. 2). These Figs. agree with each other and are both based on extensive high quality observations by Cram and Damé (1983). The Figs. show that the bright K_{2V} emission peaks only develop on the violet wavelength side. At the moment where the bright K_{2V} peak is seen, its position is near the line center ($\Delta\lambda \approx 0$) and the central K_3 absorption is red shifted. About a quarter period (≈ 40 *s*) later, the K_{2V} peak has vanished and the K_3 absorption has moved to the line center or even slightly to the violet side. From there K_3 moves slowly back to the red side starting a new cycle.

The K_2 and K_3 evolution is acompanied by a characteristic behaviour of the inner wings of the line. Roughly at the time where the K_{2V} peak is maximal, brightening starts in the wing simultaneously near ± 3 Å. This brightening subsequently moves towards the line center simultaneously from both sides and vanishes with the K_{2V} flash. As the edge of the brightenings towards the relatively darker line center is abrupt, this behaviour has also been described as symmetrical "dark whiskers" which contract to the line center.

While Deubner (1991) deduces from the waveform of the 8542Å line of Fleck and Deubner (1989), that there is no evidence for significant shocks in the K_2 layer, Kalkofen (1989, 1990,

Send offprint requests to: P. Ulmschneider

1991), following Liu (1974), sees in the cell grains a propagating wave phenomenon which heats the chromosphere by shocks; in Kalkofen (1989) these waves supposedly run up magnetic flux tubes, while in the later papers that scenario is discarded and the waves are supposed to be of purely hydrodynamic origin. In this picture the closeness of the 3 min waves to the cut-off period at the temperature minimum ($P_A \approx 180\ s$) is a problem because these waves do not propagate much energy up from the convection zone. Kalkofen considers the heating by 3 min waves as so significant, that he dismisses short-period acoustic waves (with $P < 60\ s$) as an unimportant heating process of chromospheres. We do not believe this latter opinion and have summarized the evidence for the existence of short-period acoustic waves and of their significance as heating mechanism for the low and middle chromosphere elsewhere (Ulmschneider, 1990, 1991). Indeed the mechanism discussed in the present paper can only occur if short-period acoustic waves are present.

Another point of dispute has been the question whether the horizontal localization of the cell grains is due to a magnetic field: that cell grains could be the manifestation of magnetic flux tubes. This has been claimed by Sivaraman and Livingston (1982), Sivaraman (1991). However, higher resolution work and a vanishing of the 3 min oscillation near network elements have shed doubt on this picture such that most workers consider now the cell grains to be a non-magnetic phenomenon (Deubner, 1991, Rutten and Uitenbroek, 1991).

For a long time the three-minute oscillations have been explained as a standing mode generated by a cavity between the temperature minimum and the transition layer temperature rise (e.g. Leibacher et al. 1982). Recently Fleck and Schmitz (1991) by analytical and numerical computations have shown that the three-minute oscillation is better interpreted as a cut-off frequency oscillation. Other than cavity modes this global resonance occurs as a result of an imbalance between two forces, the weight of the atmosphere and the compression of the gas. The cut-off frequency oscillation thus is a pulsational oscillation, in which the entire atmosphere is alternatively compressed and expanded with little energy transport, and in the ideal case has a phase shift of 90^0 between velocity and temperature fluctuations valid for a standing wave phenomenon.

In our present work we want to show that short-period acoustic waves can generate 3 min type phenomena and that they are able to produce a core evolution pattern very similar to that of the observed Ca II K_{2V} cell grains. This new pulsation-type phenomenon fits into the picture of Fleck and Schmitz (1991). In addition we believe that our process has great significance also for oscillations on other stars, particularly in red giants. In Sec. 2 we give a short description of our method of calculation. Sec. 3 presents the results of our wave calculations. A discussion is given in Sec. 4 and Sec. 5 summarizes our conclusions.

2. Method

2.1. The hydrodynamic computation

The computation of acoustic waves has been discussed in previous papers of this series (Ulmschneider et al. 1977, 1987, Schmitz et al. 1985) and needs therefore not to be described again. It suffices to say that the time-dependent hydrodynamic equations and the radiative transfer equations in the H^- continuum and the Mg II k line (as a representative chromospheric emitter, assuming complete redistribution CRD) are solved simultaneously with the statistical equilibrium equations for the NLTE populations using the method of characteristics. With this method the development of the originally sinusoidal wave, introduced at the bottom of the atmosphere by a piston, is followed until shock formation. At the top of the atmosphere a transmitting boundary is used. The shocks are treated as discontinuities which are allowed to grow to arbitrary strength and permitted to overtake one another. By time-independent means a pure H^- NLTE radiative equilibrium atmosphere was produced to serve as an initial atmosphere model. An NLTE radiative equilibrium atmosphere model with Mg II k line cooling was then constructed using time-dependent means by holding the piston velocity equal to zero. This atmosphere served as a starting model in which the motions had quieted down to a few cm/s.

2.2. Modified core-saturation method

In our present work the treatment of the Mg II and Ca II line emission was considerably improved. Discussed in more detail elsewhere, these improvements are now briefly described. The core-saturation method used by Ulmschneider et al. (1987) and originally developed by Kalkofen and Ulmschneider (1984, henceforth called old method) was found to be of poor accuracy when time series of the emerging line intensity were generated. This was traced to the crude evaluation of the CRD line source function,

$$S_L = \frac{\frac{1}{2}\int\int \phi_{\mu\nu} I_{\mu\nu} d\mu\, d\nu + \epsilon\, B}{p_e + \epsilon} \quad , \tag{1}$$

where

$$p_e = \frac{1}{2}\int\int \phi_{\mu\nu} d\mu\, d\nu \quad , \tag{2}$$

is the escape probability. Here the frequency integrals are taken over the wings only, $I_{\mu\nu}$ is the specific intensity, $\phi_{\mu\nu}$ the absorption profile, B the Planck function and $\epsilon = n_e \Omega_{21}/A_{21}$ the destruction probability. n_e is the electron density, Ω_{21} the collisional- and A_{21} the Einstein spontaneous transition probability.

The problems with the evaluation of S_L in the old method comes from the computation of the intensity integral, which in addition to the line shape also affects the net cooling rate. The treatment of the core-wing separation in the old method resulted in a considerable variation of the value of the wing intensity integral from time-step to time-step at a given height. Using a more refined method to perform the wing integral and a carefully chosen optical depth parameter $\Delta\tau_\gamma$ (we took $\Delta\tau_\gamma = 1$) it was possible to greatly improve the accuracy of the core-saturation method. For the details of these modifications see Rammacher (1991a, to be published).

In addition, the core-saturation was compared to other radiation methods. These were the MULTI method by Carlsson (1986) and an operator perturbation method by Kalkofen (1985, private communication). Because these methods were not developed to permit internal boundaries, we tried to artificially incorporate the shock points into the regular height grid. In our time-dependent case the shock points move freely across the Lagrangian height grid and approach grid points arbitrarily closely. This situation is no problem for the core-saturation method. To be able to employ the above mentioned other radiation methods we incorporated the shocks into the height grid in two, increasingly bold ways, each time disregarding the front shock point: in a first case we

included the post-shock point as an additional grid point and in a second case we replaced the post-shock grid point by the post-shock point. Both manipulations led to severe convergence problems in most situations, which had to do with the fact that there is a many orders of magnitude opacity jump across the shock. As in a typical time-dependent computational run the radiative transfer and statistical equilibrium equations have to be solved several thousand times, a method which frequently runs into convergence problems can not be used. We thus found that the modified core-saturation method was a reliable, fast and reasonably accurate method for our time- dependent calculations with shocks, despite of its awkward dependence on the free parameter $\Delta\tau_\gamma$. For the details of the comparison of the radiation methods see Rammacher (1991a, to be published).

Following Rammacher and Cuntz (1991) we have also included a more realistic NLTE ionization of Mg II to Mg III as well as of Ca II to Ca III. For this purpose we have computed the radiative absorption and recombination rates using mean continuum intensities

$$J_\nu = \frac{1}{b_1(T)} B_\nu(T) \quad , \tag{3}$$

where for temperatures higher than $T = 8000\ K$ we took a fixed boundary value $T_L = 8000\ K$ and where for the hydrogen ground state departure coefficient $b_1(T)$ the expression given by Hartmann and McGregor (1980) was adopted.

The treatment of the hydrogen ionization is necessary for the computation of the electron density which enters the destruction parameter ϵ in the Mg II and Ca II line calculations. For this purpose we crudely computed the H-ionization by using an NLTE Saha equation with the above mentioned departure coefficient $b_1(T)$. However, the hydrogen ionization was not taken into account in the thermodynamics and hydrodynamics for which we assume a neutral gas.

2.3. Computation of the Ca II and Mg II line profiles

For our time-dependent calculations the CRD line source function S_L of a given time-step always served as an excellent initial estimate for the next time-step. At the first time-step or at a continuation of a previous wave calculation about 30 S-iteration steps were made in the core-saturation method while interspaced in a D-iteration about 4 S-iterations were made at regular time-steps. S-iteration we have called the Λ- type iteration in the core-saturation method where from an n'th approximation of the source function S_L the intensity is calculated, which then is used to compute with Eq. (1) the n+1'th approximation of S_L. The D-iteration is the iteration to reach a consistent solution of the hydrodynamic-, radiative transfer- and statistical equations at the new time step. About 4 D-iterations were necessary to advance the solution to the next time. The D-iteration was assumed converged when the changes in the cooling rate were smaller than 1 percent. After a wave calculation is completed the CRD line source function was subsequently used to calculate the emergent line intensity with a much more refined frequency grid (217 compared to normally 29 frequency points).

3. Results

3.1. Height dependence of the physical variables

With the numerical procedure described above a series of acoustic wave computations with periods $P = 20, 30, 45, 90\ s$ and energy fluxes $F_M = 5 \cdot 10^7, 1 \cdot 10^8, 2 \cdot 10^8\ erg\ cm^{-2}s^{-1}$ were made and Mg II and Ca II line profiles were computed. Fig. 1 shows a typical snapshot of a wave calculation with $P = 45\ s$ and $F_M = 2 \cdot 10^8 erg\ cm^{-2}s^{-1}$ with the behaviour of the temperature T, the velocity v, the pressure p, the Euler minus Lagrange height difference $x - a$, the ionization fraction X of Ca II, together with the temperature distribution T_0 and the height difference $x_0 - a$ of the starting atmosphere in radiative equilibrium, as function of height. Note that the starting atmosphere, due to the added line cooling, has a much reduced NLTE chromospheric temperature rise (Cayrel effect) which results in a slight contraction from the initial pure H^- model. This is indicated by the negative values of $x_0 - a$. Fig. 2 shows for the same phase as in Fig. 1 the destruction parameter ϵ, the escape probability p_e, the line source function S_L and the true emission fraction of the source function $B' = \epsilon B/(p_e + \epsilon)$ for the Ca II K line. Here the T distribution is displayed again to permit a detailed comparison.

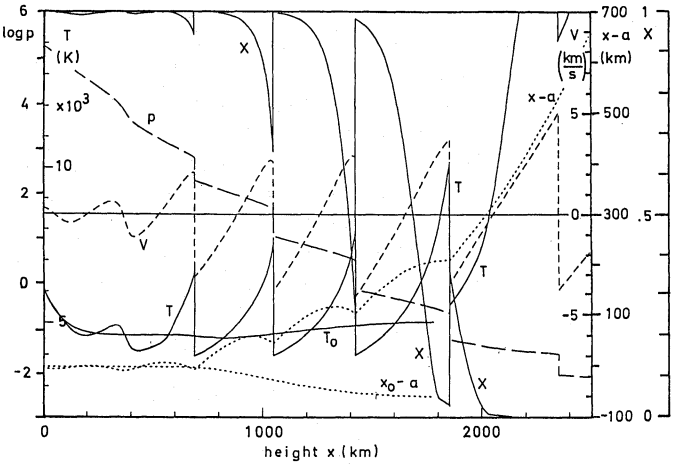

Fig. 1. Acoustic wave with period $P = 45\ s$ and initial energy flux $F_M = 2 \cdot 10^8\ erg\ cm^{-2}\ s^{-1}$ at time $t = 1065\ s$. Temperature T (K), velocity V (km/s), pressure $log\ p$ (dyn/cm^2), ionization fraction X of Ca II, Euler minus Lagrange height difference $x - a$ (km) are shown as function of Euler height x (km) together with the temperature T_0 and the height difference $x_0 - a$ of the radiative equilibrium starting atmosphere model

At about 2000 km height the temperature is seen to rise rapidly. This is a consequence of our choice to represent the entire radiative loss in the upper chromosphere by a scaled Mg II k-line emission. When the Mg II k line opacity as function of height becomes small, then the diminished line cooling leaves the shock heating unbalanced. The ionization of Mg II to Mg III at high temperature amplifies the effect even further by destroying Mg II. At the time t = 1065 s of Figs. 1,2 already 17 shocks have been transmitted at the almost adiabatic upper boundary, each raising the temperature secularly. In our time-dependent calculation this effect leads to an ever increasing steepening of the temperature rise.

This general behaviour has already been discussed by Ulmschneider et al. (1987). These authors note that the detailed

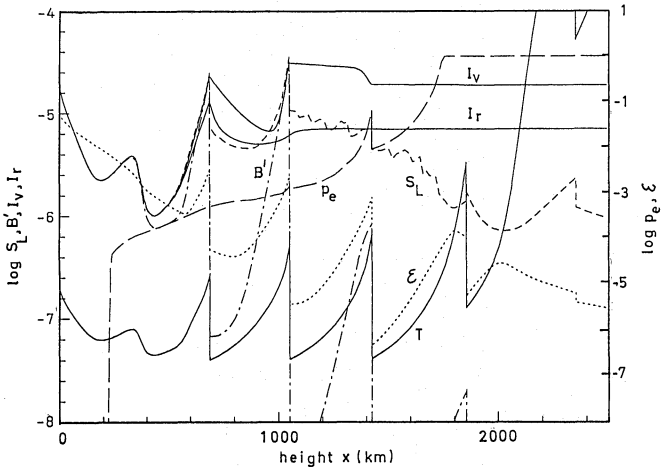

Fig. 2. Line source function S_L, its true emission fraction $B' = \epsilon B/(p_e + \epsilon)$, violet and red K2 peak intensities I_V, I_R all in $(erg/cm^2 s\ sr\ Hz)$, destruction probability ϵ and escape probability p_e as function of Euler height x for the Ca II K line and for the same wave as in Fig. 1. The temperature T is shown again for comparison, plotted on a scale as in Fig. 1

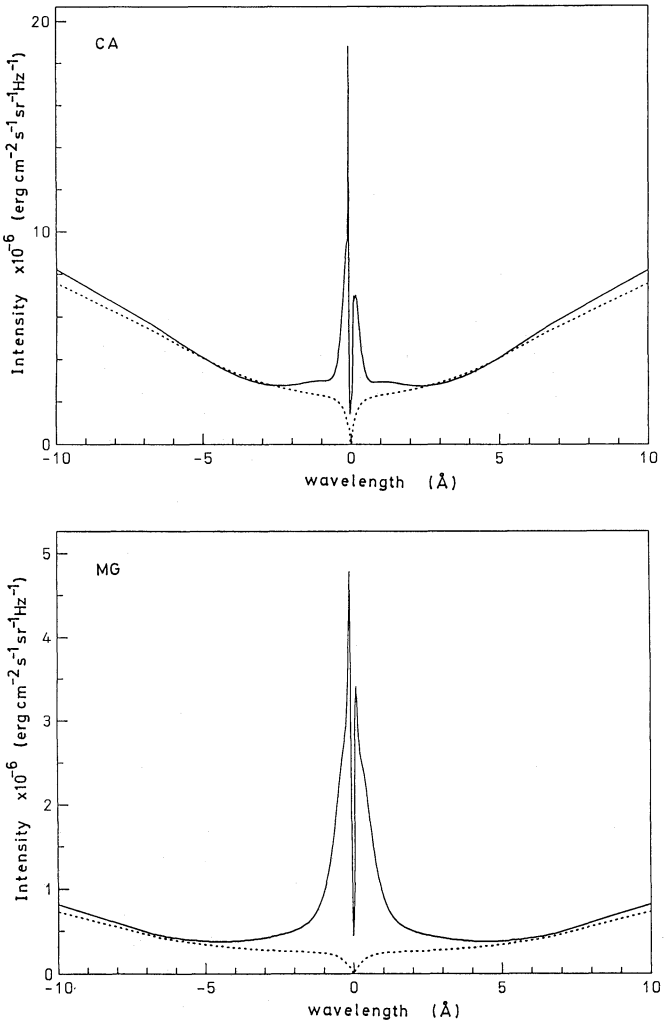

Fig. 3. Emergent Mg II k and Ca II K line intensities for the same wave as in Fig. 1 together with the intensities of the radiative equilibrium starting atmosphere

temperature rise in time-dependent calculations using H^- and Mg II as the only chromospheric emitters is unrealistic, because radiative cooling by hydrogen, in particular by the Lyman α line has been neglected, but that the temperature rise in such calculations is correct in principle, because the destruction of H I will eventually produce a similar steep temperature rise, although at somewhat greater height. A detailed treatment of hydrogen is presently beyond the scope of this work. It should be kept in mind, however, that our crude treatment of the hydrogen ionization, constitutes a considerable uncertainty in our Mg II and Ca II line computations at great height.

The behaviour of the source- and Planck functions S_L, B as well as that of ϵ and p_e for the Ca II K line is understood as follows (cf. Fig. 2). Below 400 km height LTE is seen to prevail and one has $S_L = B$. Together with the decrease of the pressure, the electron density and with it ϵ decreases with height, while the escape probability p_e, due to the increasing fraction of the frequency band which belongs to the wing (cf. Eq. (2)), increases with height and eventually reaches unity due to the normalization of $\phi_{\mu\nu}$, when the core contribution falls to zero. It is seen, that ϵ behind shocks increases due to the temperature dependence of Ω_{21} and due to the growth of n_e from the hydrogen ionization. The strong temperature dependence of the Planck function in the violet spectral range tries to pull S_L towards LTE behind the shocks (Eq. (1), see the shocks at 700 and 1050 km height in Fig. 2). At greater height ϵ has decreased so much that S_L is primarily determined by the scattering contribution and no longer follows the temperature variation.

3.2. The Mg II and Ca II line profiles

Fig. 3 shows the emerging profiles of Mg II k and Ca II K lines together with the radiative equilibrium (starting) atmosphere profiles. Both profiles show an enhancement relative to the equilibrium profiles which is due to the acoustic wave. The high outwardly increasing mean chromospheric temperature rise produced by the wave generates emission cores in the line. The most conspicuous feature is the occurrence of violet and red emission peaks, where the violet peak is consistently larger than the red peak. The low line-center intensity minimum is due to the small line source function at great height (cf. Fig. 2).

The behaviour of the Ca II line opacity of the wave of Fig. 1 is shown in Fig. 4. Ordinarily, due to the density jump of a factor of four for strong shocks we would expect an opacity jump of a factor of four at the shock discontinuity. However, as indicated by the ionization fraction X of Ca II (see Fig. 1), the high temperature behind the shocks ionizes Ca II to Ca III. While the ionization is not important at the shock at 700 km, it affects the opacity considerably behind the shock at 1050 km (see Fig. 4).

We now want to ask for the reason of the emission peak asymmetry. Consider the shock at about 1050 km height. The source function S_L behind the shock, due to the temperature sensitivity of B, rises strongly (Fig. 2) as already discussed above. The opacity behind the shock due to the approaching velocity peaks strongly at the violet side (Fig. 4), which results in a much larger optical depth on the violet, rather than on the red side. The intensity, the integral of the source function over the optical

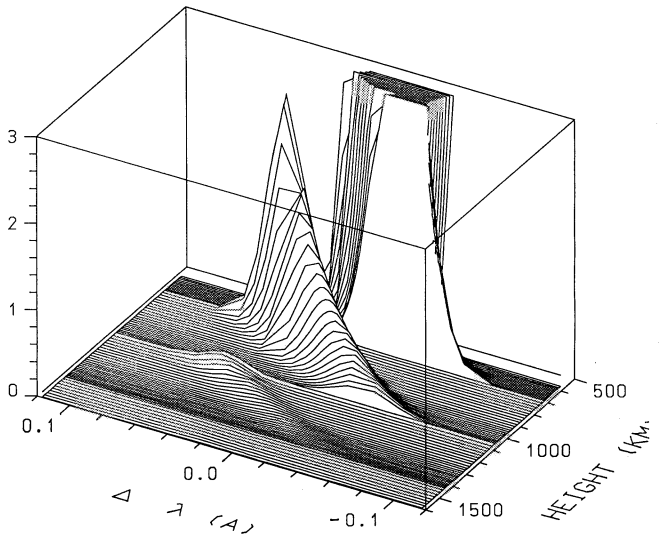

Fig. 4. Opacity κ_ν ($10^{-3} cm^{-1}$) as function of wavelength $\Delta\lambda$ (Å) and height x (km) for the same wave as in Fig. 1

depth, thus rises strongly on the violet, but only weakly on the red side. This, by the same reasoning is also found for the shock at 700 km height. On the post-shock side the violet intensity thus is larger than the red intensity.

In front of the shock the opacity mountain, because of the strongly receding velocity, is shifted out of the way of the violet intensity (Fig. 4) resulting in unobstructed radiation towards greater height (Fig. 2). Only when the violet intensity meets the next opacity mountain, shifted into the violet frequency range by the post-shock region of the shock at 1400 km height, does it decrease again and reaches its boundary value in front of this shock.

The low red intensity of the shock at 1050 km height, in outgoing direction, immediately meets an opacity mountain shifted into its frequency range by the strongly receding velocity in front of the shock (Fig. 4). Here, the intensity increases and saturates to the low value of the source function in front of the shock. As soon as the opacity mountain moves out of the way at greater height the red intensity reaches its boundary value. The red opacity of the front shock region of the next shock at 1400 km is too low to further affect the red intensity (Fig. 2). The intensity of the K_3 central absorption which is closely tied to the source function reaches its boundary value at 1800 km height.

From the above the reason why the violet K_{2V} intensity is much larger than the red K_{2R} intensity becomes clear: it is the velocity-temperature correlation in the post-shock region combined with the removal of the violet opacity in the front- shock region. It is also clear that asymmetric emission peaks are a general feature of acoustic shock waves and because the violet intensity in the post-shock region is dominated by ϵB, the temperature sensitivity of this peak is much greater than that of the red peak (see also Figs. 5). The enhancement of the violet relative to the red peak was found to be more pronounced for increasing wave period. This is explained by the fact that the strength of the shocks increases with wave period. Stronger shocks lead to larger temperature and velocity amplitudes and thus to larger temperature-velocity correlations. For a more detailed discussion of wave induced emission peak asymmetries in the Ca II and Mg II lines see Rammacher (1991b, to be published)

3.3. Time development of the Mg II and Ca II line profiles

Figs. 5 show the temporal behaviour of the Mg II and Ca II line intensities for a series of acoustic wave calculations. In order to display the differences in the line profiles more easily, we plot only the violet and red emission peak intensities as well as the central minimum intensity. The violet peak and the central minimum are indicated solid, while the red peak is shown dashed. It is seen that the emission peaks in the different wave cases behave very differently. For the $P = 90\ s$, $F_M = 1 \cdot 10^8\ erg\ cm^{-2} s^{-1}$ wave (Figs. 5a,b) the intensity oscillation clearly follows the wave period. The intensity oscillation of the $P = 45\ s$, $F_M = 2 \cdot 10^8\ erg\ cm^{-2} s^{-1}$ wave shown in Figs. 5c,d also largely follows the wave period, except near the start of the computation, where a rapidly decaying oscillation of large amplitude with a period near 3 min, best seen in the Mg II line, superposes the wave period.

The 3 min phenomenon becomes dominant for the $P = 30\ s$, $F_M = 2 \cdot 10^8\ erg\ cm^{-2}\ s^{-1}$ wave (Figs. 5e,f), where except for the red Ca II peak the wave period is no longer visible. This 3 min phenomenon is also seen in a wave with much lower energy flux as shown in Figs. 5g,h for a $P = 30s$, $F_M = 5 \cdot 10^7\ erg\ cm^{-2} s^{-1}$ wave. Here the wave period is more clearly visible in the Ca II line. In addition it is seen that the 3 min phenomenon persists over a long time although with a very noisy amplitude. Finally, Figs. 5i,j show a wave case with $P = 20s$, $F_M = 2 \cdot 10^8\ erg\ cm^{-2} s^{-1}$. Here the 3 min phenomenon is again dominant together with other long-period fluctuations, while the wave period is no longer seen in the intensity fluctuation. However, sharp intensity spikes in Mg II tell of the underlying short- period wave. In this simulation the violet and red peaks of the Ca II line are often not detected anymore. To indicate such situations we have artificially set the emission peak intensity equal to zero in Fig. 5j and other Figs.

This new 3 min phenomenon caused by short-period acoustic waves, as we will show below, is due to a pulsation of the chromosphere. We want to call it *3 min pulsation*. As the physics of the solar 3 min oscillation and that of the Ca II K_{2V} cell grains is not yet fully understood we provisionally treat all three processes as different in this work.

The comparison of the simulations in Figs. 5 clearly shows that the visibility of monochromatic acoustic shock waves in the intensity fluctuations decays rapidly with decreasing wave period and that a limit of detectability is somewhere near 30 s. This confirms similar results found for sinusoidally shaped acoustic waves and supports the validity of the modulation transfer functions determined for these waves (Langhanki, 1986, see also Deubner et al. 1988). The reason for this sharp decrease of the visibility of intensity fluctuations for shorter wave periods is that near 30 s the wavelength of the acoustic wave becomes smaller than the width of the line forming region (contribution function width). However, as discussed above, the 3 min pulsations often create favourable situations where, indicated by sharp spikes, much shorter period shocks can be seen.

Fitting parabolas to our emission peaks and evaluating the frequency of the point of zero slope we were looking for velocity fluctuations in the emission peaks. We found that the velocity was fairly constant in those phases where the violet peak had its maximum in the 3 min cycle, while at other times velocity oscillations following the wave period clearly showed. Similarly to the intensity fluctuations, the amplitude of this wave velocity

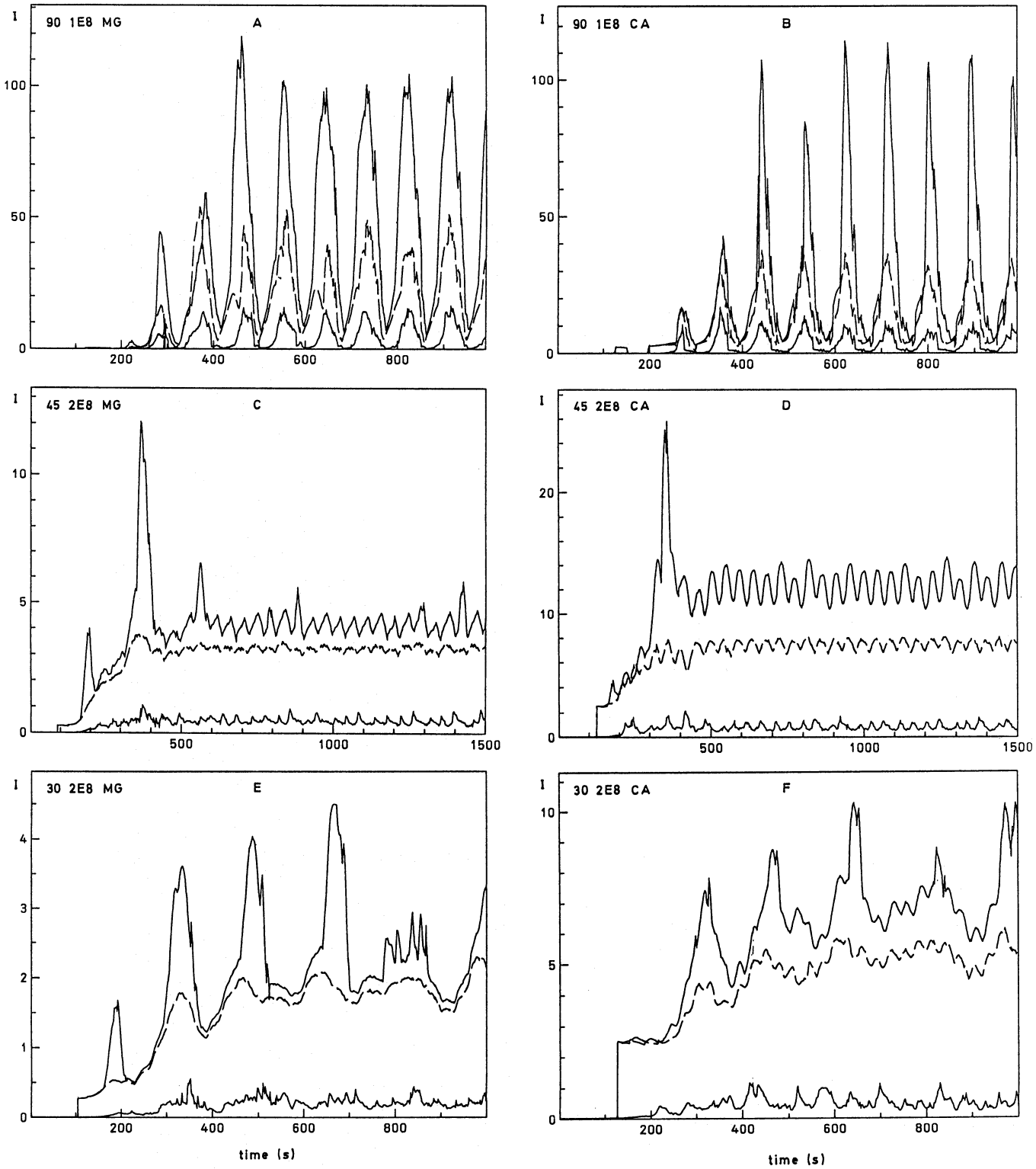

Fig. 5. Panels A-F. Emergent Mg II k and Ca II K line intensities (in units of $10^{-6} erg/cm^2\ s\ sr\ Hz$) of the violet (drawn) and red (dashed) emission peaks and the central absorption core (drawn) as function of time for various wave calculations of specified period P (s) and initial wave flux F_M ($erg\ cm^{-2}s^{-1}$). Panels A,B: $P = 90, F_M = 2 \cdot 10^8$, C,D: $P = 45, F_M = 2 \cdot 10^8$, E,F: $P = 30, F_M = 2 \cdot 10^8$, G,H: $P = 30, F_M = 5 \cdot 10^7$, I,J: $P = 20, F_M = 2 \cdot 10^8$

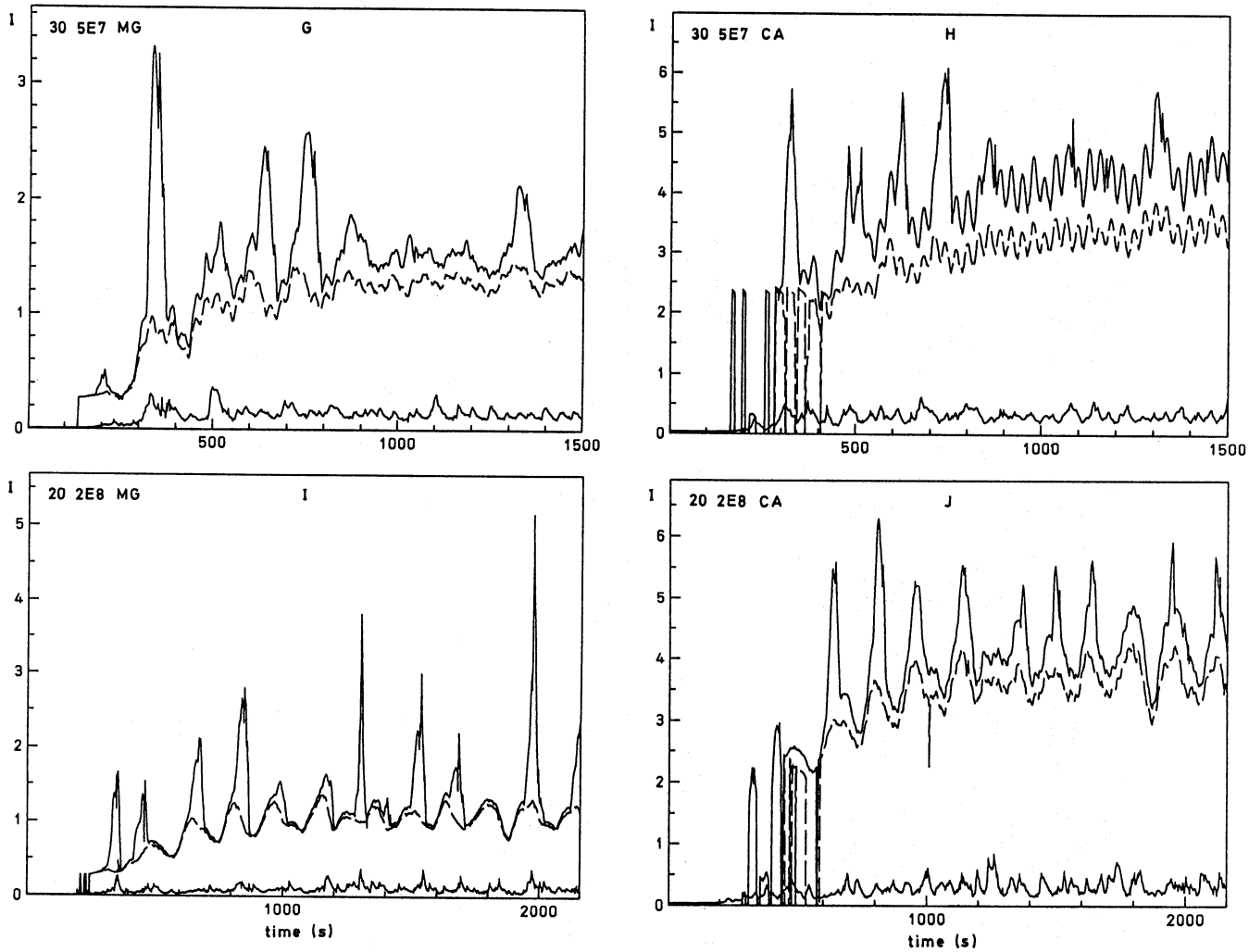

Fig. 5. Continued, panels G-J

signature decreases rapidly from the 90 s to the 30 s wave and is no longer visible for the 20 s wave. The reason why the velocity stays constant in the maximum intensity phase is that there the source of the intensity is one particular shock. Here the post-shock emission is Doppler-shifted by a constant amount because of the almost constant velocity amplitude behind the shock during its propagation.

3.4. The relation to the acoustic cut-off frequency.

For the pulsation periods we find average values of $P = 185, 164, 146, 164$ *s* in Figs. 5c, 5e,f, 5g,h, and 5i,j, respectively. For an additional calculation with a $P = 30$ *s*, $F_M = 1 \cdot 10^8$ *erg* $cm^{-2}s^{-1}$ wave, a mean pulsation period $P = 165$ *s* was found. The actual pulsation periods are seen to be quite variable, ranging from 120 to 240 s. It is interesting to compare the pulsation periods with the acoustic cut-off period which describes the fundamental vibrational resonance of the chromosphere.

$$P_A = \frac{4\pi c}{\gamma g} \quad , \tag{4}$$

where c is the sound speed, $\gamma = 5/3$ the ratio of specific heats, and $g = 2.736$ cm/s^2 the solar gravity. For temperatures of $T = 4000, 6000, 8000$ *K* we find cut-off periods of $P_A = 180, 220, 254$ *s*, respectively. Despite of the variability of the pulsation periods we interpret their difference to P_A as an indication that the two phenomena are different. Indeed we will show below that our 3 min pulsation very likely is a first overtone pulsation for which shorter periods are expected compared to the pulsation period P_A of the fundamental mode.

3.5. The Ca II and Mg II cell grain evolution

Before we turn to a more detailed description of the physics of the 3 min intensity fluctuations let us compare our computations with observations. Figs. 6 show the typical temporal evolution pattern in the first 700 s of the Mg II and Ca II line center intensities for the $P = 30$ *s*, $F_M = 2 \cdot 10^8$ *erg* cm^{-2} s^{-1} wave. Every tenth time-step is shown (it is instructive to compare Figs. 6 with 5e,f). These Figs. should be compared with the observed temporal evolution pattern of the K_{2V} cell grains (Fig. 2 of Deubner, 1991 and Fig. 2 of Rutten and Uitenbroeck, 1991) based on the observations of Cram and Damé (1983). Figs. 6 (most easily seen in the Mg II line) show how at time $t \approx 200$ *s* a strong violet peak develops and that about 40 s later after the violet peak has vanished the central absorption has shifted to the wavelength position of the

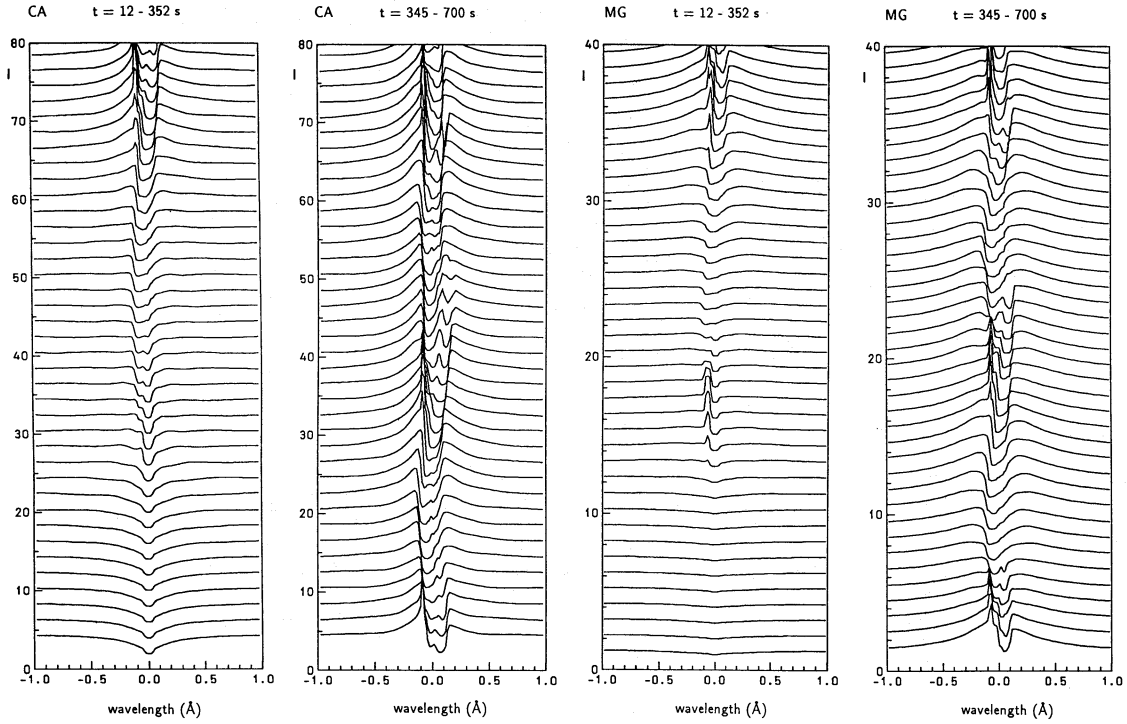

Fig. 6. Emergent Mg II k and Ca II K intensities (in units of $10^{-6} erg/cm^2\ s\ sr\ Hz$) of the line cores for the wave of $P = 30\ s, F_M = 2 \cdot 10^8\ erg\ cm^{-2} s^{-1}$, shown for every 10 time steps between times $t = 12\ s$ and 700 s. The time steps are roughly equidistant

vanished violet peak. Subsequently a new violet peak develops and pushes the central absorption back over the line center to the red, from where after the new violet peak has vanished, it moves back towards the violet side again, repeating the previous cycle. Without a detailed analysis we feel that the evolutionary pattern of our line profiles agree fairly well with the Ca II K line observations described by Deubner as well as Rutten and Uitenbroek.

3.6. Physics of the three minute pulsation

The appearance of 3 min pulsations is a new phenomenon in our acoustic wave calculations which Figs. 5 show to be associated with transients generated from the onset of the wave computations and which is suspected to be a pulsation-type phenomenon of the atmosphere. Let us now turn to the physical process which leads to the 3 min pulsation. Figs. 7a-d show the velocity v, the temperature T, the Euler-Lagrange height difference $x - a$, and the outgoing specific intensity of the violet Ca II K-line emission peak for four phases of our $P = 30\ s$ and $F_M = 2 \cdot 10^8\ erg\ cm^{-2}\ s^{-1}$ wave calculation. The four consecutive phases 7a-d are about 40 s apart in time (at 336, 382, 417, 460 s) and are chosen such that, by going back to phase 7a, the 3 min cycle is completed and the variation of the physical variables roughly indicated. The fact that our 3 min phenomenon is a pulsation-type oscillation is most easily seen in the velocity.

At heights larger than 1500 km in phase 7a, the mean velocity is strongly negative (downward) with an amplitude of -6 km/s, which is close to the sound speed of about 7 km/s, while in phase 7b it has become positive (upward) with an amplitude of +3 km/s. The mean velocity increases further to a maximum amplitude of about +7 km/s at phase 7c, from which it reverses again to negative amplitudes of -3 km/s at phase 7d and somewhat later to a maximum negative velocity similar to phase 7a, concluding the 3 min cycle.

Figs. 7 also show the associated displacement $x - a$ of the mass elements which react with a phase delay to the velocity behaviour. $x - a$ is the difference between the actual height in the laboratory frame (Euler height, x) and the original position in the initial atmosphere (Lagrange height, a). The initial atmosphere, where we had $x = a$, was a pure H^- model with a sizeable chromospheric temperature rise due to the Cayrel effect. The added Mg II line emission results in a cooler chromospheric temperature distribution in our radiative equilibrium starting model which leads to $x - a < 0$ (see Fig. 1). The $x - a$ values in Figs. 7 show three different effects. The persistent acoustic wave heating leads to an average chromospheric temperature rise, to which the atmosphere adjusts itself. This is a secular effect, resulting in a new dynamic equilibrium distribution $x - a$, which below 1400 km height is reached at the time of Fig. 7b. At the top of the atmosphere such an equilibrium cannot be attained because in our calculation no Mg II cooling is left there which leads to unrestricted heating and persistent expansion. The second effect is the lifting and subsequent falling caused by the transit of individual shocks during the 30 s wave period. This produces periodic excursions with a wavelength of about 210 km. The third effect is the 3 min type phenomenon of the atmosphere where material e.g. near 1500 km during the 3 min cycle is seen to be lifted by $\approx$ 100 km and falls back. This cycle is also apparent at much greater height but here is seen to be superposed by the mentioned persistent outward motion.

Note the phase delay in the behaviour of $x - a$ at 1500 km height and at the top of the atmosphere. While in phase 7a at 1500 km the difference $x - a$ is smallest and reaches a maximum

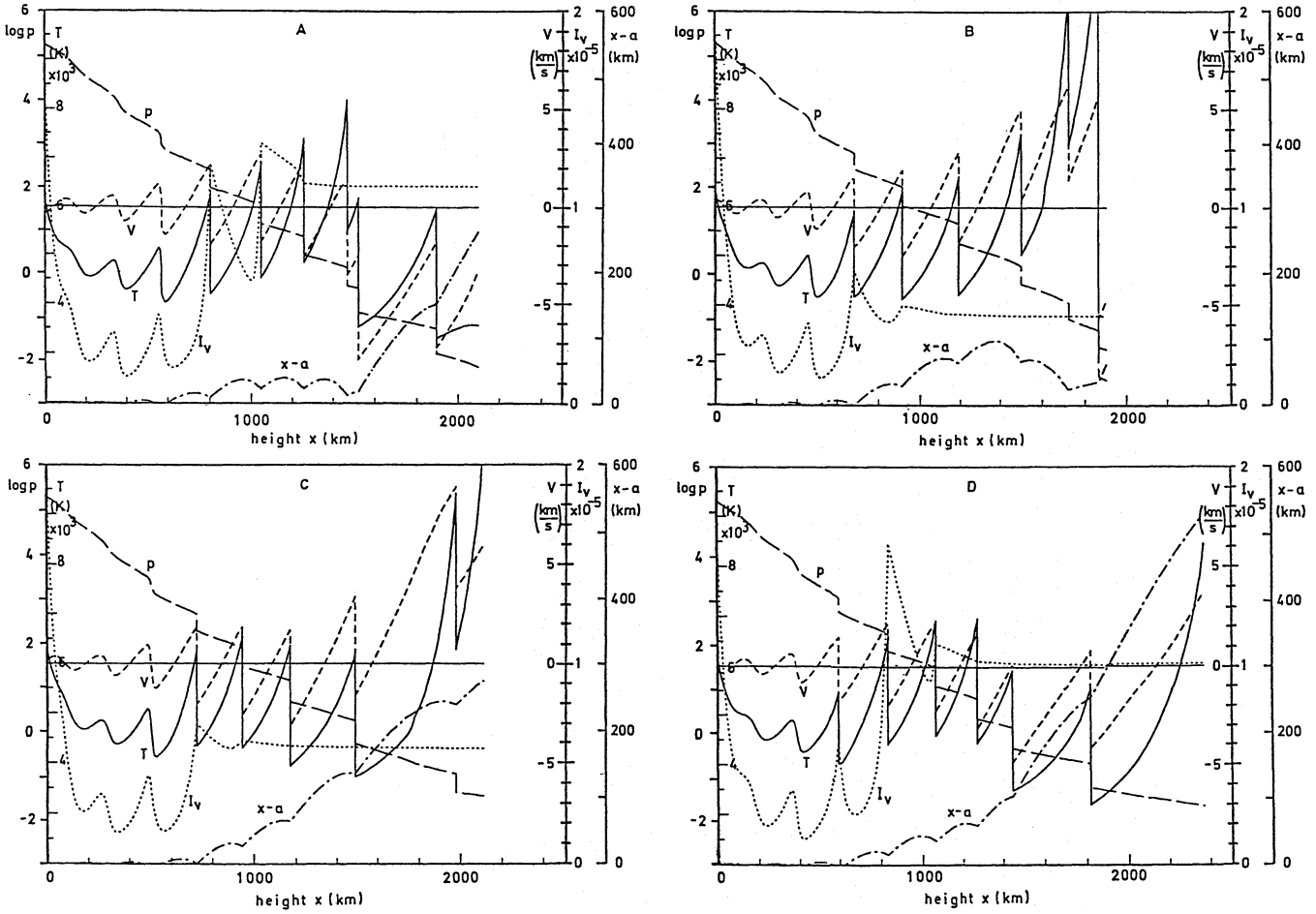

Fig. 7. Snapshots of four phases of an acoustic wave with period $P = 30$ *s* and initial energy flux $F_M = 2 \cdot 10^8$ *erg* cm^{-2} s^{-1}. Temperature T (K), velocity V (km/s), pressure $log\ p$ (dyn/cm^2), Euler minus Lagrange height difference $x - a$ (km) are shown as function of Euler height x (km). The times t are for panel A: 336 s, B: 382 s, C: 417 s, D: 460 s

at phase 7c, the difference $x - a$ at the top has its smallest value at phase 7b and its maximum at phase 7d. This phase delay is due to the propagation time of the strong shock. In phase 7d, where $x - a$ has a maximum at the top, the region near 1500 km has already contracted considerably which leads to an adiabatic heating below 1500 km and cooling above that height.

It is instructive to see the motions described above as a superposition of a short and a long wavelength phenomenon. As there is no easy way to separate the short-period wave from the 3 min phenomenon we resort to a rather crude method to affect a separation. Connecting the midpoints of the shock jumps of velocity and temperature allows to crudely determine the mean velocities and temperatures as function of height. These mean values for our four phases 7a-d are shown in Fig. 8.

Fig. 8 shows three important properties of the 3 min phenomenon. First, this phenomenon is not a fundamental but a first overtone pulsation with a node roughly in the 1200 to 1400 km height range. This is seen from the mean velocities which near 1300 km height in phase *a* and *c* cross and which in phases *b* and *d* have a maximum positive and negative amplitude, respectively. But this is also seen from the mean temperature. The temperature wave displayed in Fig. 8 rides on top of the time-independent chromospheric temperature rise which extends

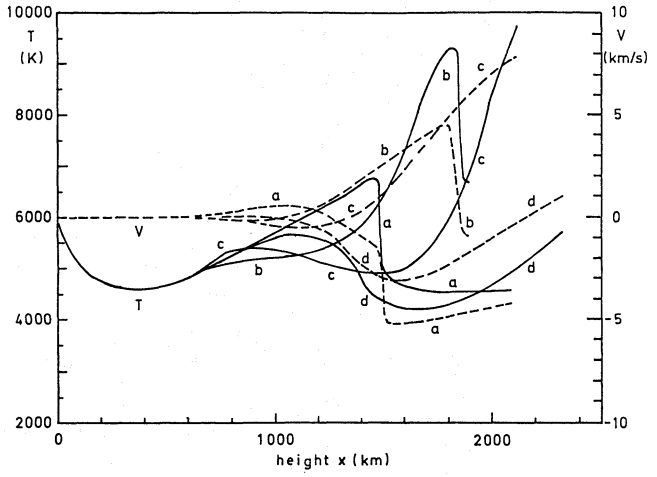

Fig. 8. Mean values of temperature and velocity for the four phases of Figs. 7a to 7d, labeled accordingly

roughly from the temperature minimum through the point at 1300 km height where the mean temperatures of phases *b* and

d cross. At this height, therefore, the mean temperature behaves similar to the velocity: the temperatures cross in phases *b* and *d* and in phases *a* and *c* have their maximum positive and negative amplitude, respectively.

The second important property of our 3 min phenomenon is that the velocity and temperature fluctuations are 90^0 out of phase in the sense that the temperature maximum in phase *a* leads the outward velocity maximum in phase *b*. The third important property is that, due to the generation of the strong shock, the phase shift between temperature and velocity decreases to zero at greater height. This behaviour of our 3 min phenomenon agrees, with the running wave picture of Liu (1974) and Kalkofen (1991). As in our case the mechanical energy input is exclusively in the form of short-period acoustic waves, it is important to recognize that the energy of the propagating 3 min wave must come entirely from nonlinear mode-coupling. To explain the observations therefore it is not necessary to postulate 3 min wave propagation up from the convection zone

Let us now consider the mode-coupling mechanism. From Figs. 7a-d it is seen that the wave, once shocks have formed, has fairly constant amplitude away from the regions where overtaking has just occured. This is consistent with the tendency of acoustic waves in gravitational atmospheres to attain a limiting strength which is determined exclusively by the wave period (Ulmschneider 1990). Due to the variations of the mean atmospheric temperature from adiabatic heating and cooling caused by the 3 min pulsation, however, there are considerable differences in the propagation speeds of the shocks in different regions of the chromosphere. In Fig. 7a below 1200 km height the mean temperature is roughly 6500 K, while at heights above 1300 km it is 4500 K. This leads to a sound speed of 8.3 km/s at low heights and 6.9 km/s at great heights. The sound speed difference is the cause of the overtaking process. A sound speed difference of 1.4 km/s leads to a displacement of the fast shock relative to the slow shock by 220 km in 3 min, which is the distance of a wavelength. Shock overtaking generates large shocks, which then vigorously (see Fig. 7b) propagate into the downflowing material, leading to the expansion phase of the 3 min pulsation. From the above we conclude that shock overtaking is the process by which the short-period wave energy is transfered into the 3 min pulsation and thus constitutes its driving mechanism.

We now come to the cause for the intensity cycle of the emission peaks. In Figs. 7a-d the intensity of the violet peak is plotted as function of height. It is seen that the source of the intensity is the hot backside of the shocks. Because of the rapidly decreasing opacity, the violet Ca II emission peaks originate in a height range of 800-1200 km (1100-1500 km for Mg II) which is similar to that of the red peak. The emerging intensity in phase 7a is behind its maximum and in phase 7d just before its next maximum.

There are two reasons for the occurrence of an emission maximum. First, the mean temperature in the region near 1000 km height, where the violet peak is emitted, is highest (see the shock near 1000 km height). Second, the mean velocity in the same region is largest (Fig. 8). An inspection of $x - a$ in Figs. 7 shows that the maximum K_{2V} emission occurs at the phase when after a considerable contraction the atmosphere around 1000 km now expands again. At great height near 2000 km where the central K_3 absorption is produced, however, the downflow is still in full swing and leads to a strongly redshifted K_3 feature seen in Fig 9a.

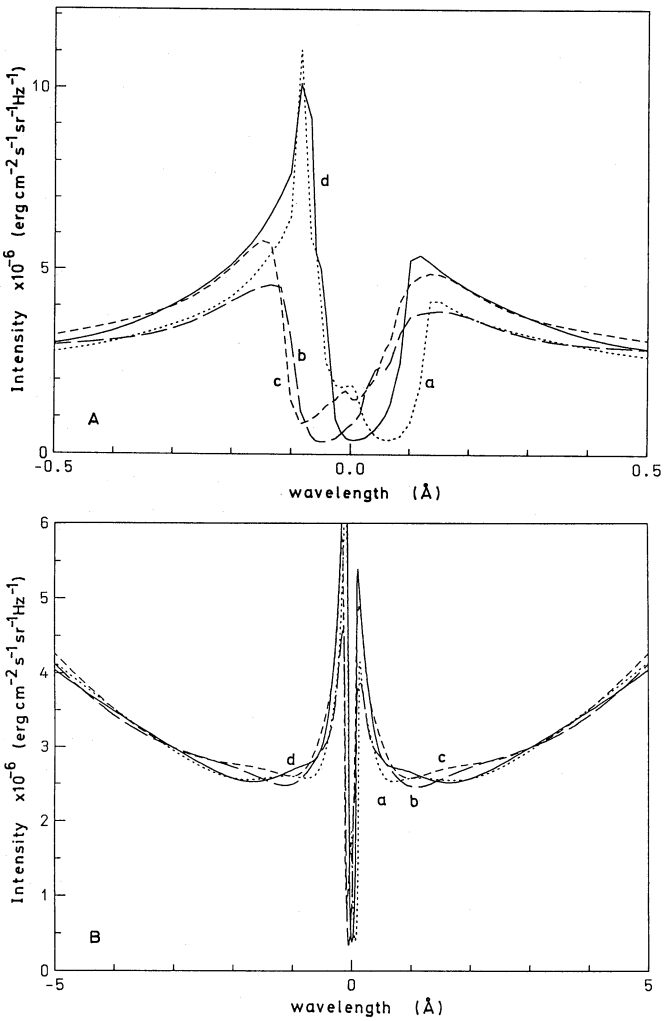

Fig. 9. Ca II K line profiles of four phases of Figs. 7a to 7d, labeled accordingly. To emphasize core and wing regions the line profiles are plotted differently in panels A, B

Shortly thereafter the shocks, by overtaking, have created a strong shock which reverses the downflowing motion in the highest layers as well, leading to a violet shifted K_3 absorption (Fig. 7b). At that phase the expansion near 1000 km height has cooled the atmosphere, greatly reducing the violet emission peak. To show the line core evolution of the phases 7a- d more clearly, Fig. 9a shows a superposition of the corresponding four emergent Ca II line profiles (see also Fig. 6).

3.7. The shock-overtaking pulsation mechanism

The process described above has similarities to the well-known κ-mechanism (Kippenhahn and Weigert, 1990, p.411) which is responsible for pulsations of Cepheid-type stars. In the Cepheid pulsation the increase of pressure and temperature due to the contraction of the outer stellar envelope increases the opacity which traps the outflowing radiation and heats the envelope. This heating reverses the contraction and leads to the expansion of the envelope. The outward motion is eventually halted because the expansion cooling undercuts the support of the outer envelope, which leads to a contraction again.

In our case the same pulsational motions occur, although not in the fundamental mode. However, our energy source is not the flow of radiation, but instead the flow of mechanical energy, in particular, acoustic shock waves. The adiabatically contracting inner atmosphere raises the temperature which leads to a faster shock propagation. The faster shocks overtake the slower shocks propagating in the adiabatically expanding downflowing outer atmosphere and generate strong shocks which reverse the downflow. This shock overtaking, by which the mechanical energy flow is modulated, is the analogue of the opacity in the κ-mechanism. Because shock overtaking lies at the core of our mechanism it might be called *shock overtaking pulsation* or sop-mechanism.

It is interesting to determine roughly the amount of energy converted from the short-period waves into the 3 min pulsation. From the fact that for waves with $P = 30,\ 20\ s$ there are 1, 2 shock overtakings per 3 min cycle we estimate that the mode conversion efficiency is 36, 50%, of the limiting acoustic flux at the overtaking height, respectively. This is because 2, 4 out of 5.5, 8 (=165 s/P) shocks combine their strength by overtaking, respectively.

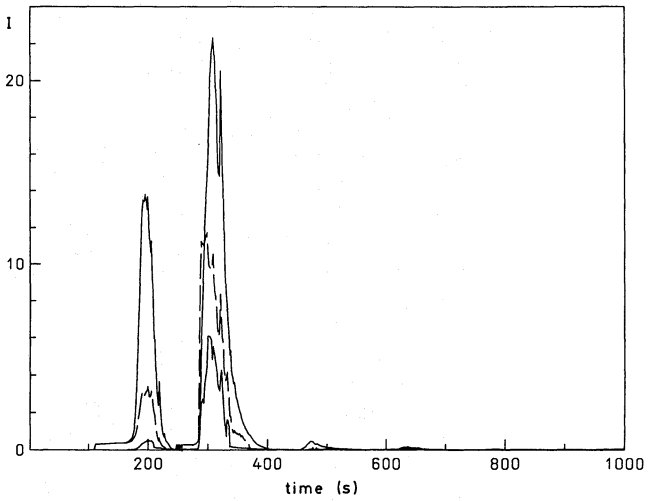

Fig. 10. Emergent Mg II k-line intensity (in units of $10^{-6} erg/cm^2\ s\ sr\ Hz$) of the violet (drawn) and red (dashed) emission peaks and the central absorption core (drawn) as function of time for a pulse calculation with an initial wave flux $F_M = 1 \cdot 10^7\ erg\ cm^{-2}\ s^{-1}$ and duration $P = 90\ s$

3.8. The dependence on the wave period

From the above discussion, particularly from Figs. 5, it is obvious that the sop-mechanism does not work for waves of all periods. Naturally all wave calculations generate transients when the calculation is switched on. Here the first shock runs into an undisturbed atmosphere and grows to a strong shock which expands the atmosphere much more than the eventual dynamical equilibrium state. The subsequent contraction from this overexpansion leads normally to a few pulsational adjustment cycles of the 3 min type which should not be confused with a driven 3 min pulsation.

One might think that the switch-on of wave calculations in a radiative equilibrium atmosphere model is very unrealistic compared to real stars. However, it has to be kept in mind that the acoustic wave energy hardly emerges in the form of monochromatic waves but, due the generation in a turbulent convection zone, is certain to arrive in the form of wave packets. Transients, therefore, are constantly occuring in realistic situations. There is no problem to do computations of waves with stochastically changing periods (e.g. Cuntz 1990). The reason why in this series of papers we use monochromatic waves in our computations is, that we want to understand the influence of the wave period.

The transients in the 90 s wave calculation of Figs. 5a,b are quickly damped. This was confirmed by following the $x - a$ behaviour as function of time. To show this quick damping even more drastically, we have performed a calculation of a wave *pulse* of $P = 90\ s$, $F_M = 1 \cdot 10^7\ erg\ cm^{-2} s^{-1}$ which we have produced by stopping the piston motion after one wave period. Fig. 10 shows the Ca II emission peak intensity behaviour as function of time. It is seen that similarly to the 90 and 45 s wave calculations (see Figs. 5a, 5c) the transients get quickly damped.

The reason for this is the wavelength. The first overtone pulsation generates a sound speed gradient which results in a difference in the shock propagation speeds. Only waves with periods as short as about 30 s have small enough wavelength, that it is possible for the shocks to overtake each another. For 45 s waves the overtaking occurs (if it does!) high in the atmosphere and thus is unimportant for the Ca II and Mg II line forming layers.

This reasoning is confirmed by our 20 s calculations. Waves with such periods dissipate very rapidly and grow only to small amplitude. The switch-on transients generated by such waves are thus quite small. However, the initial adjustment pulsations, which occur when the radiative equilibrium atmosphere responds to persistent mechanical heating, get rapidly amplified by the many shock overtakings which generate large shocks. Figs. 11 give two illustrative examples 83 s apart. Comparisons of Figs. 11 with Figs. 1 and 7 show the small limiting strength shock amplitude of the 20 s wave relative to that of the 45 s and 30 s waves. Fig. 11a shows that two shock overtakings are about to occur generating strong shocks which in turn lead to large flows in the upper chromosphere as seen in Fig. 11b. Yet a comparison of Figs. 5i,j with 5e,f shows that despite of the growth of the 3 min pulsation the Ca II and Mg II emission peak intensity fluctuation is not very vigorous, due to the small limiting acoustic flux carried by the 20 s wave.

To summarize, it appears that the sop-mechanism works only for wave periods below 40 s such that overtaking is possible in the chromosphere. For a wave period near 30 s the mechanism has a large effect, because the wave carries a relatively large energy flux. For even smaller periods the overtaking mechanism is more efficient, but the pulsation is smaller.

3.9. Dependence on the acoustic flux, the Ca II line core evolution again

We now want to discuss how the wave energy affects the 3 min pulsation. Consider once more the line core profile evolution of the $P = 30\ s$, $F_M = 2 \cdot 10^8\ erg\ cm^{-2}\ s^{-1}$ wave of Fig. 6. Let us compare this evolution with that of the wave with $P = 30\ s$, $F_M = 5 \cdot 10^7\ erg\ cm^{-2}\ s^{-1}$ shown in Fig. 12. It is seen that in the wave with less energy the 3 min pulsation is still present, which has already been shown in Figs. 5g,h. The large Doppler motion of the central K_3 absorption feature of Fig. 6, however, is not seen in Fig. 12. Likewise, the violet emission peak evolution is less variable. Moreover, in both Figs. 6 and 12 the typical Doppler motion of the K_3 core and the variability of the violet emission peak appear greater in the Mg II line than in the

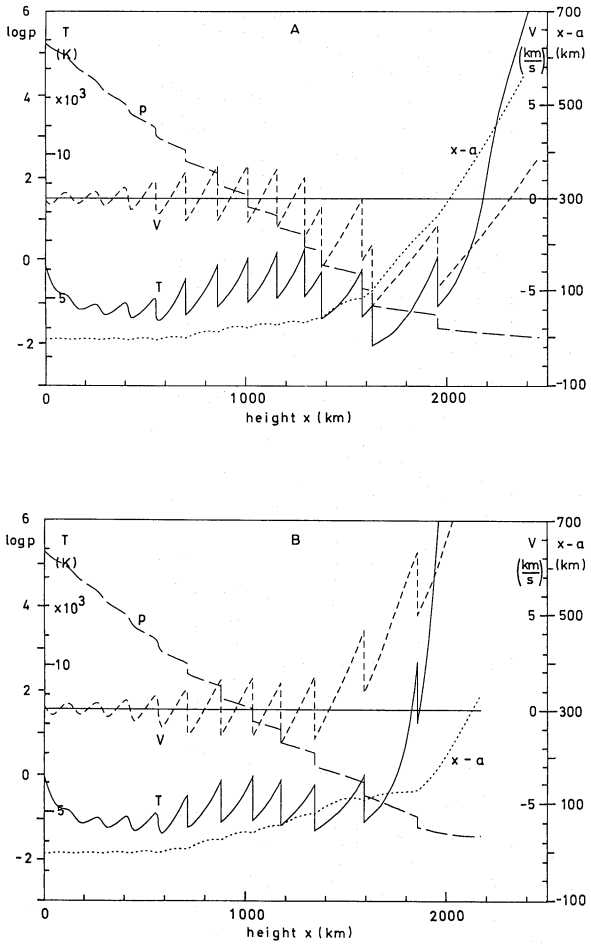

Fig. 11. Snapshots of two phases of an acoustic wave with period $P = 20\ s$ and initial energy flux $F_M = 2 \cdot 10^8\ erg\ cm^{-2}\ s^{-1}$. Temperature T (K), velocity V (km/s), pressure $log\ p$ (dyn/cm^2), Euler minus Lagrange height difference $x - a$ (km) are shown as function of Euler height x (km). The times t are for panel A: 968 s, B: 1051 s

Ca II line. This in our view has to do with the dependence of the acoustic waves on energy. For a given wave period, a wave with large energy flux forms shocks at lower height compared to waves which small flux. For our 30 s wave with fluxes of $F_M = 5 \cdot 10^7, 1 \cdot 10^8, 2 \cdot 10^8\ erg\ cm^{-2}\ s^{-1}$, shock formation occurs at 500, 750, 1000 *km* height, respectively. A half wavelength above these heights the waves reach the same limiting strength in the three cases.

As the process of shock overtaking occurs only, when the shocks are fully developed, the sop-mechanism for the wave of higher initial energy flux will thus operate in a lower, denser atmospheric region and as a consequence, the atmospheric flows at great height will be more violent. A lowering of the acoustic energy flux thus reduces the magnitude of the pulsation. As the overtaking height determines the mass involved in the pulsation we expect also that the pulsation period varies with the wave energy. This was indeed found in Sec. 3.4, where the wave of Figs. 5g,h has a much smaller pulsation period $P = 146\ s$ than the wave of Figs 5e,f with $P = 164\ s$. Another noticeable effect is that because for smaller period the limiting strength shock wave has lower energy, our 20 s wave generates a smaller effect than the 30 s wave (compare Figs. 5e,f with 5 i,j). Finally, because the Mg II line is formed in a 200 km higher region, a more violent pulsation is present there, than in the much denser Ca II line formation region.

3.10. The inner wing behaviour

In their review Rutten and Uitenbroek (1991, Sec. 2.1.1) list three characteristic properties of the K_{2V} cell grains. Two of these, the K_{2V} flashes and the K_3 manoeuver can be fairly well reproduced by our computations (see our Sec. 3.5). The third characteristic property is the symmetric wing brightening migration towards the line center (or alternatively the dark whisker contraction). Fig. 9b shows the the wings of the simulated Ca II K line for the four atmospheric situations of Figs. 7. The phases *a* to *d* again label the situations shown in Figs. 7a to 7d, respectively. It is seen that shortly after the K_{2V} flash, phase *a* shows a symmetric brightening at ± 4 Å, which at phase *b* has propagated to ± 1.5 and at phase *c* to ± 1.2 Å. The spectral speeds agree roughly with those quoted by Rutten and Uitenbroek. However, there remain puzzling discrepancies. Figs. 9 show a relatively large K_{2R} emission peak, which is not seen in the observations. It will be shown below (Sec. 4.2) that this red emission peak could be an artifact of the use of complete redistribution in our calculations.

4. Discussion

4.1. Uncertainties due to the computational domain and the monochromatic spectrum

Before we discuss the relationship between our 3 min pulsations and the 3 min oscillations more broadly we first want to mention a few limitations of our work. The computations of acoustic waves in a radiative equilibrium solar model reported above show that a pulsational phenomenon occurs which is driven by large shocks generated by shock overtaking. It is clear that shock overtaking is more likely if the distance to the next shock is small, that is, for small wave periods. As for a greater extent of the atmosphere, longer period shocks will overtake one another, it is obvious that our results could depend on the size of the computational domain. The size of our chromosphere model is determined by the height of the transition layer temperature rise which in turn is determined by the optical depth in the Mg II line, because, as discussed above, if Mg II becomes optically very thin, then our shock heating becomes unbalanced. Shock overtaking is not very likely to happen in the transition layer. There, by distributing the wave energy over a rapidly increasing wavelength due to the rising sound speed, the wave amplitude and consequently the non-linear effects decrease. The error in the size of our computational domain thus depends on how realistic our transition layer is determined. This in turn hinges on the treatment of Lyman α, which at the present time can not be done adequately.

However, to produce the observed emission core evolution in the Ca II line, the shock overtaking should happen as low as about 1500 km, as happens for our $P = 30\ s$, $F_M = 2 \cdot 10^8\ erg\ cm^{-2}\ s^{-1}$ wave and not at 1800 km as in the wave with $P = 30\ s$, $F_M = 5 \cdot 10^7\ erg\ cm^{-2}\ s^{-1}$. Even overtaking heights of 1800 km are well inside our computational domain. From this we conclude that a better treatment of the high chromosphere

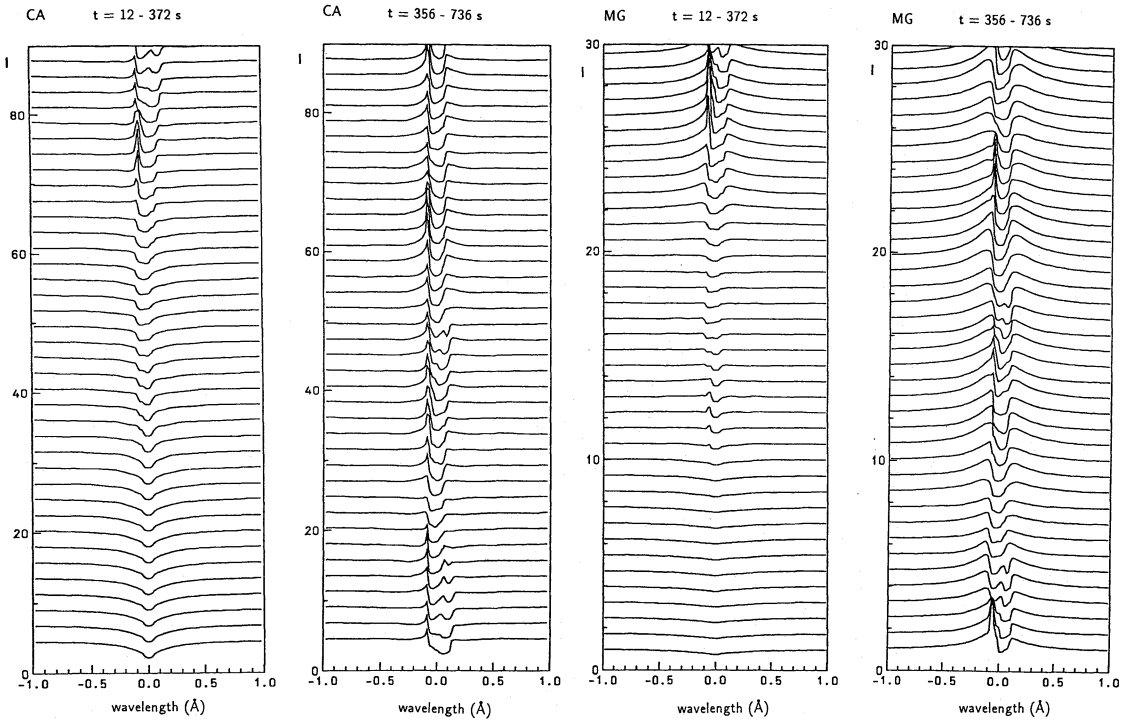

Fig. 12. Emergent Mg II k and Ca II K intensities (in units of $10^{-6} erg/cm^2\ s\ sr\ Hz$) of the line cores for the wave of $P = 30\ s, F_M = 5 \cdot 10^7\ erg\ cm^{-2}\ s^{-1}$, shown for every 10 time steps between times $t = 12\ s$ and 736 s. The time steps are roughly equidistant

will not alter much our finding that the 3 min pulsation needs short-period waves with periods less than 40 s.

Another criticism may be our use of monochromatic waves. As already discussed above, the choice of monochromatic waves in our computations was necessary to investigate the dependence on the wave period, but is not very realistic, because the acoustic energy very likely emerges from the convection zone in the form of wave packets. The behaviour of the sop-mechanism in a stochastic wave field will be discussed in a subsequent paper. The shocks which happen to be in the hot contraction region are those which eventually overtake the slow shocks in the expansion region. This shows that the coherence length of the wave does not need to be very long, and that the effect does not depend on some ratio of the pulsation period to the wave period. Our result, that the pulsation is more vigorous when the wave has more energy, which we attribute to a deeper shock overtaking height, points to some dependence of the pulsation period on the overtaking height. We will address this point in a subsequent paper.

4.2. Emission peak asymmetry and our use of CRD

In our calculations, particularly in cases of strong shocks, generated by large wave periods or by overtaking, we found that the use of complete redistribution (CRD) causes errors which leads to unrealistic enlargements of the red emission peaks. In Fig. 2 the source function S_L in front of the shock near 1050 km height after Eq. (1) is primarily due to the scattering term. In the scattering term there are contributions from both the red and the violet line intensity. Because the violet intensity behind the shock is much larger (see Sec. 3.2) it is the dominant contribution for the scattering term. For partial redistribution (PRD) this cross scattering of the violet intensity over roughly 5 Doppler widths would give vanishing contribution for the red spectral region. A frequency-dependent PRD source function will thus be much smaller on the red side. The large frequency-independent CRD source function in front of the shock, in turn, leads to an unrealistic growth of the red intensity (see Fig. 2). A correct PRD treatment thus would considerably lower the red source function and reduce the red intensity significantly. This effect, which we presently are unable to treat, would result in a greater violet-red emission peak asymmetry, which would be in better agreement with observations (Rutten and Uitenbroek, 1991).

4.3. The relationship with the three minute oscillations

Let us now discuss how consistent our pulsation-type motions, generated by short-period shock waves, are with the observations. We have already seen that the emission core evolution in simulated Ca II and Mg II lines is very similar to the observed K_{2V} cell grain evolution patterns. As our sop- mechanism generates 3 min type propagating waves in the chromosphere we are also in agreement with the main observational point by Liu (1974) and Kalkofen (1989, 1990, 1991), without having to assume that the 3 min waves travel up from the convection zone. As the mode-conversion efficiency from the short-period waves is large, the 3 min waves have considerable energy to heat the high chromosphere. The frequency spectrum of our 3 min pulsations which peaks near 165 s agrees with that found by Liu (1974) although the difficulty with the missing treatment of Lyman α and a realistic transition layer prevents us from generating long time series to improve our statistics. In addition, particularly if realistic wave packets of different periods are envisioned, our mechanism would generate a relatively broad 3 min spectrum

where the fundamental pulsation modes discussed by Fleck and Schmitz (1991) will also be excited. We thus envision that the fundamental and first overtone pulsations are both present.

There remains the problem with the phase relationships observed by Fleck and Deubner (1989) in the Ca II infrared triplet (IRT) lines (for additional relevant discussions see Rutten and Uitenbroek, 1991). From our Figs. 7 it is clear that our line formation is very different from that in smooth monotonous atmospheres which is the basis for the analysis of the Deubner group. As the Ca II emission is strongly concentrated behind the shocks, we would expect a strongly spatially correlated emission of the IRT lines. Unfortunately we did not have a multilevel Ca II line simulation code which worked satisfactorily for our strongly shocked atmospheres. A preliminary result using Carlsson's MULTI code (see Sec. 2.2) to simulate the IRT lines over one 3 min cycle, did indeed show a high correlation of the core motions of the IRT lines. If the difference in the formation heights of the IRT lines were greatly decreased, then Deubners standing wave picture would have to be revised. The IRT line phase question thus must await more detailed Ca II multi- line simulations for realistic atmospheres with strong shocks.

Another important observation of Fleck and Deubner (1989) is the 90^0 phase shift between velocity and intensity fluctuations of the same line which is found for all Ca II IRT lines. As already discussed above, it is difficult to see 30 s waves in the observations, because of the width of the line contribution function. Thus only the mean longer period behaviour will be seen. The mean behaviour of our computations near 1300 km height, as discussed in Sec. 3.6 and as shown in Fig. 8, indeed shows the 90^0 phase shift in the correct orientation, with temperature leading velocity.

An additional observational fact which we should explain is the high spatial localization of the observed K_{2V} grains. It has already been pointed out long ago by Kuperus (1972, see also Kuperus, 1991) that the acoustic energy generation is by no means homogenous over the solar surface. It is therefore possible that the 3 min pulsations arise only where the short-period acoustic wave generation happens to be particularly large.

4.4. Comparison with other acoustic wave calculations

Because Rutten and Uitenbroek (1991) have discussed in detail the many attempts to simulate the observed K_{2V} cell grain behaviour we do not need to repeat it here. They classify the attempts in three classes, ad hoc models, acoustic wave and shock train simulations. From their simulation using ad hoc models they find that the K_3 behaviour can only be reproduced if large velocities with supersonic velocity steps are used. This agrees with our velocities.

Acoustic wave models do not give enough K_{2V} versus K_{2R} asymmetry, tend to produce similar violet and red emission peaks together with a rather weak K_3 behaviour. Shock wave trains give a better K_{2V} flash property but show the limiting shock strength tendency which leads to amplitudes which are too small to explain the K_3 behaviour. As the amplitude of limiting strength shocks is larger for greater wave period, long-period shocks were better to simulate the K_3 behaviour, but even these waves were found to produce an insufficient effect (Gouttebroze 1989).

The simulations using ad hoc velocities, temperatures and phase shifts are useful in rough studies but are a dangerous procedure in detail because the fact that the acoustic energy must propagate from the convection zone and that acoustic waves possess characteristic nonlinear properties (shock formation, limiting shock strength behaviour and shock overtaking) cannot be taken into account.

The reason why even realistic previous shock calculations failed is due to the neglect of the process of shock overtaking. Only by shock overtaking is it possible for acoustic waves to propagate from the convection zone and to generate strong shocks and large, even supersonic velocities in the chromosphere. However, as discussed above, significant shock overtaking only happens for waves with periods of less than 40 s.

4.5. Properties which must be discussed in greater detail in future work

In this present paper we did not discuss in detail how the 3 min spectrum looks like and what the magnitude of the radiation damping of the 3 min pulsation is. In such a discussion the difference between a pure transient (e.g. a $P = 90$ *s* pulse) and a driven 3 min pulsation would become clearer. Such investigations, with phase plots in the pressure- volume diagram, will be addressed in a subsequent paper. A discussion of the energy transfer to pulsation type motions would also be important for other stars than the sun, in particularly for late-type giant stars, where acoustically driven mass loss appears to be a promising mechanism but only, when the wave period is large (Cuntz 1990).

5. Conclusions

1. We find that short-period acoustic shock waves by the process of shock overtaking are able to drive 3 min type pulsations in the solar chromosphere. This mechanism which has similarities to the κ-mechanism in Cepheid pulsations may be called shock overtaking pulsation (sop) mechanism. As the shock overtaking process depends on the temperature difference between the hot contraction and cool expansion regions of the pulsation, it is a first overtone and not a fundamental oscillation.
2. The 3 min pulsations generated by acoustic waves may be an explanation for the observed Ca II K_{2V} cell grains. The simulated emission core evolution of the Ca II K and the Mg II k lines for our wave calculations agree fairly well with the observed emission core properties of the K_{2V} cell grains, the K_{2V} flash, the large K_{2V}-K_{2R} asymmetry, the K_3 Doppler evolution which involves large velocities and the symmetric wing brightening behaviour.
3. The predominance of the violet emission peak is due to the correlation of high temperature with high approaching velocity behind the shock and the severe weakening of the opacity in the violet spectral region due to the receding velocity in front of the shock. The asymmetry in our work is still too small due to our use of complete redistribution which leads to unrealistically large red emission peaks.
4. Shock overtaking occurs only if the wavelength of the shock wave is small enough, such that the excess speed of the faster moving shock is able to catch up with the slower shock within the chromosphere. We find that the 3 min pulsation can only be driven by waves with periods below 40 s. This finding is independent of the wave energy, due to the limiting strength property of shock waves which leads to similar shock speeds.
5. Higher wave energy, which produces shock formation at lower chromospheric height, leads to a more violent 3 min pulsation.
6. The shock overtaking pulsation mechanism transfers a considerable amount of energy (of the order of 35-50 percent of the available short-period wave flux) into the 3 min pulsation which

has the appearance of a propagating wave. This agrees with a running 3 min wave picture.
7. The shock overtaking pulsation process, by feeding energy into long-period waves may be very important for the driving of mass loss in red giant stars.
8. The discrepancies between our 3 min pulsation process and the observations by Fleck and Deubner (1989) who favour a standing wave picture can probably be resolved by calculating realistic Ca II IRT line heights. We find a similar 90^0 phase shift between temperature and velocity near 1300 km height as that found by Fleck and Deubner. Our present work suffers from a simplistic treatment of the high chromosphere, the importance of which is difficult to assess. Here the treatment of the Lyman α line cooling is urgently needed.

Acknowledgements. The authors want to thank the Deutsche Forschungsgemeinschaft for generous provision of funds for project Ul 57/11-2, and thank Dr. Rob Rutten for careful reading of the manuscript.

References

Carlsson, M.: 1986, Report No. **33**, Uppsala Astron. Obs.
Cram, L.E., Damé, L.: 1983, *Astrophys. J.* **272**, 355
Cuntz, M.: 1990, *Astrophys. J.* **353**, 255
Deubner, F.-L.: 1991, in: *Mechanisms of Chromospheric and Coronal Heating*, P. Ulmschneider, E.R. Priest, R. Rosner Eds., Springer, Berlin, p. 6
Deubner, F.-L., Fleck, B.: 1990, *Astron. Astrophys.* **228**, 506
Deubner, F.-L., Reichling, M., Langhanki, R.: 1988, in: *Advances in Helio- and Asteroseismology*, IAU Symp. **123**, J. Christensen-Dalsgaard, S. Frandsen Eds., Reidel, Dordrecht, p.439
Fleck, B., Deubner, F.L.: 1989, *Astron. Astrophys.* **224**, 245
Fleck, B., Schmitz, F.: 1991, in: *Mechanisms of Chromospheric and Coronal Heating*, P. Ulmschneider, E.R. Priest, R. Rosner Eds., Springer, Berlin, p. 22
Gouttebroze, P.: 1989, *Astrophys. J.* **337**, 536
Hartmann, L., McGregor, K.B.: 1980, *Astrophys. J.* **242**, 260
Kalkofen, W.: 1989, *Astrophys. J. (Letters)*, **346**, L37
Kalkofen, W.: 1990, in: *Basic Plasma Processes on the Sun*, IAU Symp. **142**, E.R. Priest, V Krishan Eds., Kluwer, Dordrecht, p. 197
Kalkofen, W.: 1991, in: *Mechanisms of Chromospheric and Coronal Heating*, P. Ulmschneider, E.R. Priest, R. Rosner Eds., Springer, Berlin, p. 54
Kalkofen, W., Ulmschneider 1984, in: *Methods in radiative transfer*, W. Kalkofen Ed., Cambridge Univ. Press, p. 131
Kippenhahn, R., Weigert, A.: 1990, *Stellar Structure and Evolution*, Springer, Berlin
Kuperus, M.: 1972, Solar Phys. **22**, 257
Kuperus, M.: 1991, in: *Mechanisms of Chromospheric and Coronal Heating*, P. Ulmschneider, E.R. Priest, R. Rosner Eds., Springer, Berlin, p. 343
Langhanki, R.: 1988, unpublished Diplom thesis, Univ. Würzburg, Germany
Leibacher, J.W., Gouttebroze, P., Stein, R.F.: 1982, *Astrophys. J.* **258**, 393
Liu, S.-Y.: 1974, *Astrophys. J.* **189**, 359
Rammacher, W., Cuntz, M.: 1991, *Astron. Astrophys.* in press
Rutten, R.J., Uitenbroek, H.: 1991, *Solar Phys.* **134**, 15
Schmitz, F., Ulmschneider, P., Kalkofen, W.: 1985, *Astron. Astrophys.* **148**, 217
Sivaraman, K.R.: 1991, in: *Mechanisms of Chromospheric and Coronal Heating*, P. Ulmschneider, E.R. Priest, R. Rosner Eds., Springer, Berlin, p. 44
Sivaraman, K.R., Livingston, W.C.: 1982, *Solar Phys.* **80**, 227
Ulmschneider, P., Kalkofen, W., Nowak, T., Bohn, U.: 1977, *Astron. Astrophys.* **54**, 61
Ulmschneider, P., Muchmore, D., Kalkofen, W.: 1987, *Astron. Astrophys.* **177**, 292
Ulmschneider, P.: 1990, in: *Cool Stars, Stellar Systems and the Sun*, Astr. Soc. Pacific Conf. Ser. **9**, G. Wallerstein Ed., p. 3
Ulmschneider, P.: 1991, in: *Mechanisms of Chromospheric and Coronal Heating*, P. Ulmschneider, E.R. Priest, R. Rosner Eds., Springer, Berlin, p. 328

This article was processed by the author using Springer-Verlag TEX A&A macro package 1991.